

The Interlayer Method: A Universal Tool for Energy Level Alignment Tuning at Inorganic/Organic Semiconductor Heterojunctions

Thorsten Schultz,* Dominique Lungwitz, Elena Longhi, Stephen Barlow, Seth R. Marder, and Norbert Koch

The combination of inorganic and organic semiconductors in a heterojunction is considered a promising approach to overcome limitations of each individual material class. However, to date only few examples of improved (opto-)electronic functionality have been realized with such hybrid heterojunctions. The key to unraveling the full potential offered by inorganic/organic semiconductor heterojunctions is the ability to deliberately control the interfacial electronic energy levels. Here, a universal approach to adjust the offset between the energy levels at inorganic/organic semiconductor interfaces is demonstrated: the interlayer method. A monolayer-thick interlayer comprising strong electron donor or acceptor molecules is inserted between the two semiconductors and alters the energy level alignment due to charge transfer with the inorganic semiconductor. The general applicability of this method by tuning the energy levels of hydrogenated silicon relative to those of vacuum-processed films of a molecular semiconductor as well as solution-processed films of a polymer semiconductor is exemplified, and is shown that the energy level offset can be changed by up to 1.8 eV. This approach can be used to adjust the energy levels at the junction of a desired material pair at will, and thus paves the way for novel functionalities of optoelectronic devices.

due to their potential for realizing novel or improved functionality of electronic and optoelectronic devices. For instance, inorganic semiconductors typically feature high charge carrier mobility while their organic counterparts can provide for strong light-matter coupling. Through their combination it should be possible to take advantage of the beneficial properties of both material classes and, at the same time, compensate for less favorable properties of each material class in the hybrid structure. For example, the performance of solar cells based on PbSe nanocrystals and amorphous silicon was significantly enhanced by incorporation of a thin pentacene layer, in which efficient singlet fission increased the number of generated charge carriers.^[1] Further examples of the functionality of such hybrids are interfacial exciton dissociation for photovoltaic applications,^[2–5] interfacial energy transfer for color conversion,^[5–7] and hybrid charge-transfer states that

absorb and emit light in a spectral region not accessible by either component.^[3,8–10] As is the case for any semiconductor heterojunction, the interfacial electronic energy level alignment plays a key role for the function and efficiency of the resulting device. For the hybrid interface, the relevant energy levels are the valence band maximum (VBM) and conduction band minimum (CBM) of the inorganic component, and the highest occupied molecular orbital (HOMO) level and lowest unoccupied molecular orbital (LUMO) level of the organic component. The position of these energy levels with respect to each other determines whether charge injection/extraction across the interface is facilitated,^[11] energy transfer is enabled,^[5–7] or whether interfacial charge separation occurs.^[12,13] One way to modify the energy level alignment is chemical modification of the organic semiconductor. Although the tunability of the electronic structure of organic semiconductors by means of varying their chemical structure is versatile, it has its limits and may not always be sufficient to achieve the desired properties. Another approach is to adjust the work function of the inorganic semiconductor, which in turn leads to a re-alignment of the energy levels of the organic semiconductor. Surface-grafted self-assembled monolayers (SAMs) comprising dipolar phosphonic acid derivatives were used to change the work function

1. Introduction

Semiconductor heterojunctions comprising inorganic and organic components receive increasing attention in research

Dr. T. Schultz, D. Lungwitz, Prof. N. Koch
Humboldt Universität zu Berlin
Institut für Physik & IRIS Adlershof
Berlin, Germany
E-mail: tschultz@physik.hu-berlin.de

Dr. T. Schultz, Prof. N. Koch
Helmholtz-Zentrum für Materialien und Energie GmbH
Berlin, Germany

Dr. E. Longhi, Dr. S. Barlow, Prof. S. R. Marder
School of Chemistry and Biochemistry and Center
for Organic Photonics and Electronics
Georgia Institute of Technology
Atlanta, GA 30332-0400, USA

 The ORCID identification number(s) for the author(s) of this article can be found under <https://doi.org/10.1002/adfm.202010174>.

© 2020 The Authors. Advanced Functional Materials published by Wiley-VCH GmbH. This is an open access article under the terms of the Creative Commons Attribution License, which permits use, distribution and reproduction in any medium, provided the original work is properly cited.

DOI: 10.1002/adfm.202010174

of ZnO over a 1.5 eV range,^[14] and the level alignment between ZnO and the organic semiconductor *N,N'*-di(1-naphthyl)-*N,N'*-diphenyl-(1,1'-biphenyl)-4,4'-diamine (α -NPD) was tuned by 0.3 eV with different SAMs.^[9] However, the range over which the work function can be tuned with SAMs is limited, and inevitable interfacial oxide formation during SAM processing can compromise the interfacial electronic quality of non-oxide inorganic semiconductors.^[15] Substantially larger changes of the work function of inorganic surfaces have been demonstrated by using strong electron donor or acceptor molecules^[16–18] that undergo ground-state electron transfer with the inorganic compound. Depending on the direction of the electron transfer an increase or decrease of the work function occurs; the induced work function change scales with the molecular coverage and saturates at monolayer coverage.^[16,19] A significant body of work in relation to this has focused on modifying the work function of conductive electrode materials and thereby minimizing charge injection barriers into organic semiconductors,^[18,20–27] but reports on semiconductor heterojunctions are scarce.^[16,17,28] For instance, that this work function change indeed leads to a re-alignment of the interfacial energy levels was shown for ZnO and an organic blue-light-emitting semiconductor,^[17] where the pristine heterojunction exhibited efficient charge separation after optical excitation, whereas after the insertion of a monolayer of a molecular electron donor the heterojunction supported energy transfer and subsequent light emission. However, apart from a few individual examples showing how inorganic/organic semiconductor heterojunctions could be adjusted with either an electron donor or acceptor interlayer, the full potential of interfacial level tuning with this approach has not yet been validated.

Here, we demonstrate the universality of this so-called interlayer method, by showing that the level alignment of hybrid heterojunctions between inorganic and organic semiconductors can be tuned with current state-of-the-art donor and acceptor molecular interlayers over an unprecedented range of 1.8 eV. We chose silicon as the inorganic semiconductor, because it is presently still the most technologically relevant example, specifically its hydrogenated (111) surface [H:Si(111)] due to its chemical stability and inertness. Further, we chose the molecular semiconductor α -NPD, processed in vacuum by evaporation, and the polymer semiconductor poly[(9,9-dioctylfluorene-2,7-diyl)-*alt*-(benzo[2,1,3]thiadiazole-4,7-diyl)] (F8BT), processed from solution, because they are both commonly used in organic electronic devices. For interlayer formation, we selected the potent electron donor mesitylene pentamethylcyclopentadienyl ruthenium dimer ([RuCp*(mes)]₂) and the electron acceptor 1,3,4,5,7,8-hexafluoro-11,11,12,12-tetracyanonaphtho-2,6-quinodimethane (F6-TCNNQ), the chemical structures of which are shown in **Figure 1**. The combination of X-ray (XPS) and ultraviolet (UPS) photoelectron spectroscopy allowed determination of energy levels, as well as of surface band bending changes in H:Si(111) upon interface formation. The interfacial energy level alignment was accordingly determined for three scenarios: α -NPD on bare H:Si(111), and with either donor or acceptor interlayers, evidencing the capability of molecular donor/acceptor interlayers to adjust the hybrid heterojunction energy levels over a huge range. Ultimately, we even realize qualitatively different energy level scenarios for the heterojunctions, both processed either by evaporation in vacuum or from solution, opening up powerful possibilities for varying device functionalities for the same material pair.

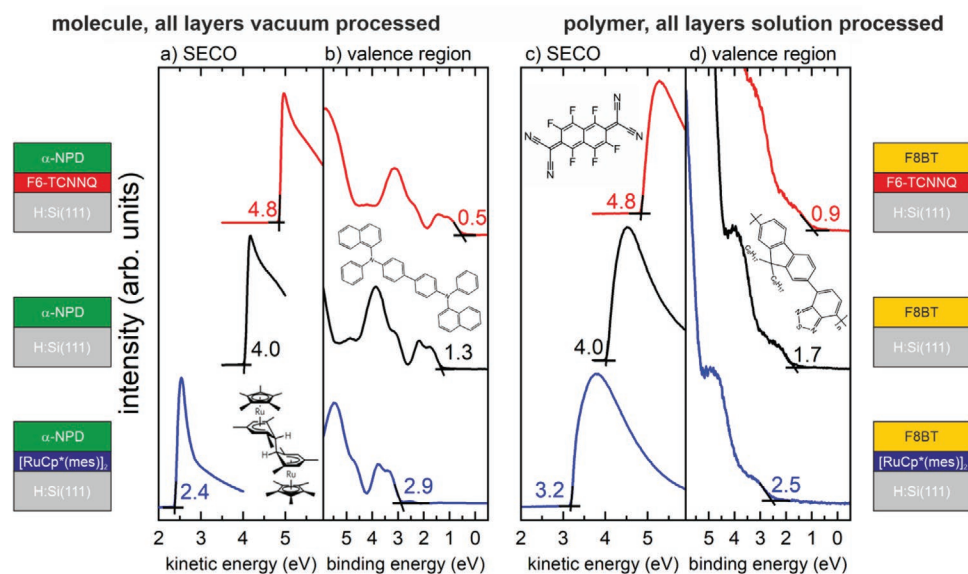


Figure 1. Ultraviolet photoelectron spectroscopy (UPS) a) secondary electron cut-off (SECO) and b) valence spectra for H:Si(111)/[RuCp*(mes)]₂/ α -NPD (blue), H:Si(111)/ α -NPD (black), and H:Si(111)/F6-TCNNQ/ α -NPD (red). The α -NPD thickness is ca. 5 nm in all cases. The work function is obtained from the SECO onsets as indicated in the figure. In b) the typical α -NPD valence region spectral shape is clearly observable for all cases. The HOMO onset of α -NPD (indicated by numbers) shifts according to the work function of donor/acceptor-modified H:Si(111), and varies between 0.5 and 2.9 eV. All films were deposited by thermal evaporation in UHV. c) and d) show analogous data for films of F8BT (thickness of ca. 4 nm) deposited by solution processing in a glovebox. The F8BT valence band (VB) onset shifts according to the Si work function change. The structures of the molecules and the polymer are shown next to the spectra, and the schematic heterojunction structures are on the right and left sides.

2. Results and Discussion

After annealing in ultrahigh vacuum (UHV), pristine H:Si(111) surfaces exhibited a work function of (4.1 ± 0.2) eV, in agreement with values reported earlier.^[29–32] A determination of the VBM position from the low binding energy photoemission onset is not readily possible from the UPS valence band spectrum (Figure S1, Supporting Information), as the silicon top-most valence band has a wide dispersion, and thus a very broad intensity distribution without a clear onset in the energy distribution curve. However, since the energy difference between the VBM and the Si2p_{3/2} core level is fixed and known to be 98.74 eV,^[33] the valence band onset position can be determined from the binding energy of the Si2p_{3/2} core level. This was determined from our samples to be between 99.1 and 99.3 eV; this range reflects typical sample-to-sample variation due to the solution-based surface hydrogenation and unavoidable short air exposure. This implies that the VBM is ca. 0.5 eV below the Fermi level (E_F) at the surface (XPS and UPS are highly surface sensitive, with the information depth being in the range of 1 nm). The bulk Fermi level of our silicon samples was calculated from the donor dopant concentration and the charge neutrality equation,^[34] which renders E_F to be 0.78 eV above the VBM, indicating that the bulk is slightly *n*-type. Consequently, there is a ca. 0.3 eV upward surface band bending in our pristine H:Si(111) due to surface states.

We start by describing the energy level alignment between silicon and α -NPD processed in UHV by evaporation. Upon evaporation of 5 nm α -NPD onto bare H:Si(111), there is no significant shift of the secondary electron cutoff (SECO) (less than -0.1 eV), that is, the work function remains essentially unchanged, which indicates vacuum level alignment (see Figure 1a), black curve). Also the Si 2p core level does not shift in binding energy (see Figure S2, Supporting Information), signifying no change of the surface band bending within H:Si(111). In the UPS valence spectra shown in Figure 1b, (black curve) the typical α -NPD spectral shape is observed, with the features corresponding to ionization from the HOMO and HOMO-1 levels centered at binding energies of 1.7 and 2.2 eV, respectively. The low binding energy onset of the α -NPD HOMO feature is 1.3 eV below E_F , yielding an ionization energy of 5.3 eV, in agreement with literature.^[35–38] Consequently, right at the interface the energy difference between the H:Si(111) VBM and the α -NPD HOMO onset is 0.8 eV. All observations point to negligible interfacial charge rearrangements within the two compounds forming the hybrid structure.

The evaporation of a nominal thickness of 1.5 nm of the acceptor F6-TCNNQ (corresponding to ca. one monolayer) onto H:Si(111) increases the work function significantly to 5.3 eV. This is due to electron transfer from silicon to F6-TCNNQ,^[39] as the electron affinity of F6-TCNNQ is higher than the work function of H:Si(111).^[19,40] This interfacial charge rearrangement increases the sample work function. The corresponding reduction of electron density in near-interface Si leads to a shift of the Si2p core level to lower binding energy by about 0.3 eV (Figure S2, Supporting Information), that is, an increase in the upward surface band bending in Si, positioning the VBM only 0.2 eV below E_F . While the bulk of the H:Si(111) is slightly *n*-doped (see above), the surface appears *p*-doped. Consequently,

the molecular acceptor deposition induces the spontaneous formation of an inversion layer near the silicon surface.

Upon α -NPD evaporation on top of H:Si(111)/F6-TCNNQ, the work function decreases with increasing α -NPD thickness (Figure S3, Supporting Information), saturating at 4.8 eV beyond 5 nm. This behavior is reminiscent of Fermi level pinning at the HOMO of α -NPD, in line with the fact that the work function of H:Si(111)/F6-TCNNQ is on par with the ionization energy of α -NPD. The low binding energy tail of the density of states from the HOMO donates electrons to the underlying high work function substrate to reach electronic equilibrium.^[41] Consequently, the α -NPD side of the junction becomes depleted of electrons, and the work function is lowered. The diffusion of surplus positive charge in the α -NPD layer away from the interface, and the associated charge density gradient, results in energy level bending, as previously explained in experiment^[42] and theory.^[43] Accordingly, we see evidence for such energy level bending away from the interface here, as indicated by a rigid shift (ca. 0.1 eV) of the UPS valence features and sample work function when going from 1 nm to 5 nm α -NPD thickness (Figure S3, Supporting Information). For the 5 nm film of α -NPD on H:Si(111)/F6-TCNNQ [Figure 1a,b, red curves] the HOMO level onset is found at 0.5 eV, in good agreement with previous values for HOMO-pinned α -NPD on other substrates.^[36,44] The surface band bending within H:Si(111), and thus the interfacial hole accumulation density, remains essentially constant (within ca. 50 meV, as judged from the Si2p core level). We thus derive an energy offset between the H:Si(111) VBM and the α -NPD HOMO onset of 0.3 eV, which is a substantial reduction compared to the value found for the heterojunction formed with pristine H:Si(111).

To decrease the work function of H:Si(111) we used [RuCp*(mes)]₂, a molecular electron donor that has been shown to effectively decrease the work function of other materials.^[17,23,45] After evaporation of ca. one monolayer [RuCp*(mes)]₂ the work function of H:Si(111) is reduced to an exceptionally low value of 2.4 eV (see Figure S4, Supporting Information). This is caused by the donation of two electrons per dimer to the H:Si(111), as the dimer dissociates into two monomeric cations upon reaction with the surface.^[46] This is accompanied by a shift of the Si2p core level to higher binding energy by about 0.5 eV (see Figure S2, Supporting Information), resulting in flattening of the Si bands at the interface, that is, the surface band bending is eliminated. This positions the H:Si(111) VBM ca. 0.8 eV below E_F . Quite notably, there is no shift of the SECO after deposition of α -NPD, that is, the work function remains constant. This implies that no further charge rearrangement occurs upon deposition of the organic semiconductor onto H:Si(111)/[RuCp*(mes)]₂, and vacuum level alignment prevails. This is expected because the electron affinity of α -NPD is ca. 1.5 eV,^[47] considerably lower than the work function of the bare H:Si(111)/[RuCp*(mes)]₂ surface. The onset of the α -NPD HOMO is found 2.9 eV below E_F , and its energy difference from the H:Si(111) VBM is a sizable 2.1 eV.

The energy levels of these three different heterojunctions are summarized in Figure 2a. Remarkably, the energy offset between the VBM of H:Si(111) and the HOMO onset of α -NPD can be tuned from 0.3 to 2.1 eV, and that between the H:Si(111) CBM and the α -NPD LUMO onset from 3.1 to 1.3 eV. This is

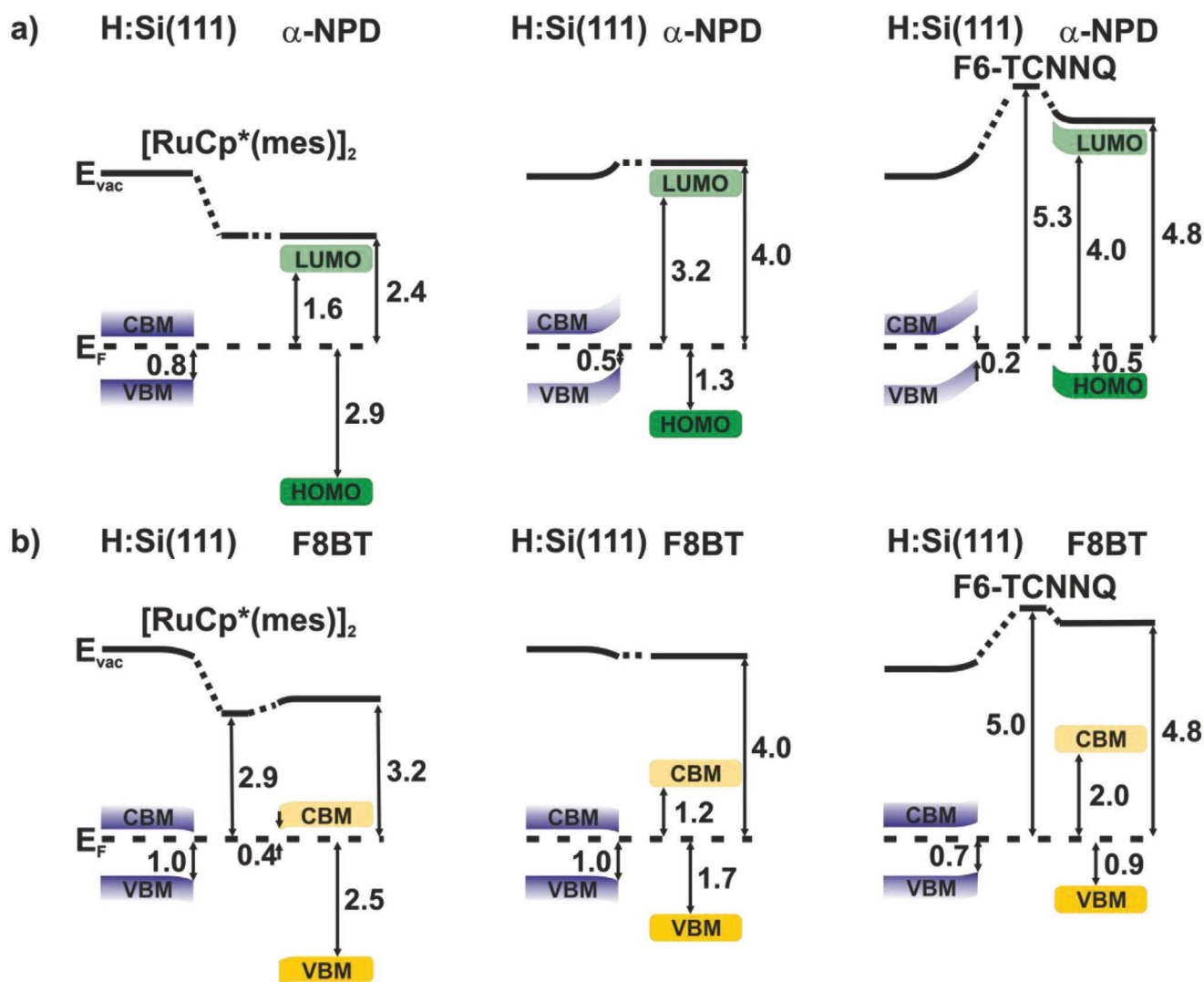


Figure 2. Detailed energy level diagrams for a) H:Si(111)/[RuCp*(mes)]₂/α-NPD, H:Si(111)/α-NPD, and H:Si(111)/F6-TCNNQ/α-NPD, and b) H:Si(111)/[RuCp*(mes)]₂/F8BT, H:Si(111)/F8BT, and H:Si(111)/F6-TCNNQ/F8BT. Si in (a) and (b) exhibits different surface band bending due to different surface preparation (see Experimental Section). The energy of unoccupied levels (CBM and LUMO) are taken from literature, and considers the transport gap of silicon, α-NPD, and F8BT.^[47,50,51]

enabled by the capacity of the molecularly thin (ca. monolayer) donor/acceptor interlayers to change the work function of H:Si(111) all the way from 2.4 to 5.3 eV. It should be noted that also virtually any work function value in between these extremes can be realized by appropriately adjusting the donor/acceptor coverage in the sub-monolayer regime, as the work function value scales with coverage.^[16,19] Accordingly, any heterojunction level alignment in between those shown in Figure 2a could also be realized. In terms of functionality, the hybrid structure changes from moderately permeable for hole transport from the organic to the inorganic side (with the F6-TCNNQ interlayer) to strongly hole blocking (with the [RuCp*(mes)]₂ interlayer), while being electron blocking from H:Si(111) to α-NPD in either situation. A closer look at the UPS spectra (Figure S5, Supporting Information) reveals that surplus electrons in the F6-TCNNQ layer at the energy of the singly occupied molecular orbital (SOMO) level are at higher binding energy than that for

the H:Si(111) VBM and α-NPD HOMO on either side, that is, they are localized within the molecularly thin interlayer. Given that SOMO levels are singly occupied (with their empty counterpart forming the singly unoccupied molecular orbital level above E_F), they should support charge transport within this 2D layer, provided that appropriate intermolecular coupling facilitates electron transfer from an anion to a neighboring neutral interlayer molecule. The strong confinement of these levels and charges on the nanometer scale in a plane is reminiscent of a charged quantum well. Upon appropriately adjusting the energy levels and coupling of the three components (inorganic and organic semiconductor, molecular interlayer) of the hybrid heterojunction it might be possible to form quasi-2D electron gases^[48] or achieve high conductivity in confined geometry.^[49]

After explaining the energy level alignment scenarios at the silicon/α-NPD interfaces in detail, we demonstrate the

universality of the interlayer method, by also tuning the energy level alignment between silicon and a polymer semiconductor, where both interlayer and polymer are processed from solution. The details of solution processing are described in the Experimental Section. After deposition of F8BT onto bare H:Si(111) no significant change of the work function is observed (Figure 1c), indicating the absence of notable interfacial charge rearrangement and vacuum level alignment. The onset of the F8BT VB is 1.7 eV below E_F (Figure 1d), resulting in an ionization energy of about 5.7 eV, in agreement with literature values.^[51] With an interlayer of F6-TCNNQ the work function after polymer deposition is 4.8 eV and the VB onset is accordingly closer to E_F (at about 0.9 eV). A solution-processed interlayer of [RuCp*(mes)]₂ reduces the H:Si(111) work function to about 2.9 eV, and it increases slightly to 3.2 eV after F8BT deposition. This indicates Fermi level pinning at the LUMO level, in line with an electron affinity of F8BT of 2.8 eV.^[51] The HOMO onset shifts to 2.5 eV below E_F , resulting in an interfacial level tuning range of 1.6 eV for F8BT. Notably, although the interlayers and polymer were deposited from solution, this is a similar range to that achieved for α -NPD processed in UHV. The energy levels of these three different heterojunctions are summarized in Figure 2b. It should be mentioned that solution processing did not result in a pronounced intermixing of interlayers and F8BT, and the donor/acceptor molecules remain essentially at the silicon surface, as evidenced by angle-dependent XPS measurements (see Figure S6, Supporting Information).

Despite the superior capacity of the interlayer method to tune heterojunction energy levels, as demonstrated by our results, we briefly discuss two limiting factors of this approach. i) The effective ionization energy (electron affinity) determines the ability of the donor (acceptor) molecules to decrease (increase) the work function of the inorganic semiconductor, and thus the amount by which the subsequently deposited organic semiconductor energy levels can be shifted. [RuCp*(mes)]₂ and F6-TCNNQ are among the strongest molecular donors and acceptors available today. They can induce work function values as low as 2.2 eV or as high as 6.3 eV,^[17,19] spanning a tremendous range of more than 4 eV. The development of even stronger donors/acceptors faces the challenge that these would be very likely to react with oxygen and/or water, making them more difficult to handle in ambient atmosphere. However, approaches like subsequent activation with light could help to further expand the range of work function modulation in the future.^[52] ii) A fundamental limitation is Fermi level pinning at the HOMO/LUMO levels.^[53] As long as the work function of the inorganic semiconductor is within the energy gap of the organic semiconductor, energy level tuning will follow the work function modification if vacuum level alignment prevails. Once the work function approaches the HOMO/LUMO level of the organic semiconductor, further increase/decrease of the work function will not lead to a further significant change of the level alignment because charge transfer pins E_F . Therefore, depending on the density of states of the organic semiconductor frontier energy levels, the HOMO/LUMO cannot approach E_F more closely than typically a few hundred meV.^[43] However, by minimizing the width of this density of states, for example, by reducing structural disorder, the range of level tuning can be maximized.

3. Conclusions

With this contribution, we revealed the full versatility of the interlayer method, which employs thin interlayers of strong donor or acceptor molecules to alter the energy level alignment at inorganic/organic semiconductor heterojunctions. The donor [RuCp*(mes)]₂ and the acceptor F6-TCNNQ allow tuning the work function of H:Si(111) between 2.4 and 5.3 eV, which in turn enabled adjusting the frontier-energy-level offset to the molecular semiconductor α -NPD by an impressive 1.8 eV. We further demonstrate the universality of the interlayer method by showing that 1.6 eV level tuning for Si and solution-processed interlayers and a polymer semiconductor is possible. The range of tuning might further be extended by the development of even stronger donors and acceptors. Beyond quantitative level tuning, we demonstrated that qualitatively very different energy level scenarios can be realized. This includes flat-band conditions on either side of the heterojunction, formation of an inversion layer within H:Si(111), and concurrent *p*-type energy level bending away from the interface within each semiconductor with spatially confined electron accumulation in the molecular interlayer. Overall, the interlayer approach is thus applicable to virtually any combination of inorganic and organic semiconductors, rendering this method a powerful tool for interface engineering in devices.

4. Experimental Section

Coupons cut from a Si(111) wafer (SIEGERT WAFER GmbH; donor doping level specified as 10^{13} – 10^{14} cm⁻³) were sonicated in isopropanol and acetone for 10 min each, before being immersed in a 40% NH₄F solution for 800 s to remove surface oxides and to saturate the remaining dangling bonds with hydrogen. Subsequently, the samples were transferred to a custom UHV system (base pressure 10^{-9} mbar) with only short time exposure to air (<5 min). They were in-situ annealed at ca. 400 °C to minimize remaining surface contamination. This step was omitted for the solution-processed films, which were directly loaded into the glovebox after ex-situ treatment. All photoelectron spectroscopy measurements were performed using an Omicron EA125 hemispherical energy analyzer with an energy resolution of ca. 150 meV. Non-monochromatized Mg K α (1253.6 eV) and Al K α (1486.6 eV) radiation was used for XPS, and He I (21.21 eV) radiation was used for UPS. A voltage of -10 V was applied between sample and analyzer during measurements of the SECO. Molecular materials were either evaporated from resistively heated quartz crucibles and the nominal deposited mass-thickness was determined with a quartz-crystal microbalance, or were deposited via the following solution process. Stock solutions with concentrations of 1 mg ml⁻¹ were prepared under nitrogen atmosphere in a glovebox using cyclohexane to dissolve F8BT, 1,2-dichlorobenzene (o-DCB) for the acceptor molecule F6-TCNNQ, and tetrahydrofuran (THF) to dissolve [RuCp*(mes)]₂. The stock solutions were stirred overnight prior to deposition. Thin film thicknesses were achieved by spin-coating at various speeds (200–1000 rpm) and times (1–2 min). It should be mentioned here that after washing of the donor/acceptor layers in the respective pure solvents the silicon work function remained unchanged in the case of F6-TCNNQ, but was still lowered to 2.9 eV for [RuCp*(mes)]₂ even without any evidence for either of the two in XPS. F6-TCNNQ was obtained from Novaled, α -NPD from Sigma-Aldrich, and [RuCp*(mes)]₂ was synthesized as described elsewhere.^[54] Cyclohexane, o-DCB, and THF were purchased as anhydrous solvents from Sigma-Aldrich GmbH (>99.5% purity, inhibitor-free).

Supporting Information

Supporting Information is available from the Wiley Online Library or from the author.

Acknowledgements

The work was funded by the Deutsche Forschungsgemeinschaft (DFG) – Projektnummer 182087777 – SFB 951 and the National Science Foundation (DMR-1807797). The authors thank Qiankun Wang for help with the silicon cleaning procedure.

Conflict of Interest

The authors declare no conflict of interest.

Keywords

energy level alignment, heterojunctions, interlayers, photoelectron spectroscopy, semiconductors

Received: November 27, 2020

Published online: December 18, 2020

- [1] B. Ehrler, K. P. Musselman, M. L. Böhm, R. H. Friend, N. C. Greenham, *Appl. Phys. Lett.* **2012**, *101*, 153507.
- [2] L. Martinez, S. Higuchi, A. J. Maclachlan, A. Stavrinadis, N. C. Miller, S. L. Diedenhofen, M. Bernechea, S. Sweetnam, J. Nelson, S. A. Haque, K. Tajima, G. Konstantatos, *Nanoscale* **2014**, *6*, 10018.
- [3] A. Panda, K. Ding, X. Liu, S. R. Forrest, *Phys. Rev. B* **2016**, *94*, 125429.
- [4] P. Ehrenreich, A. Groh, H. Goodwin, J. Huster, F. Deschler, S. Mecking, L. Schmidt-Mende, *Sci. Rep.* **2019**, *9*, 74.
- [5] S. Blumstengel, S. Sadofev, C. Xu, J. Puls, R. L. Johnson, H. Glowatzki, N. Koch, F. Henneberger, *Phys. Rev. B: Condens. Matter Mater. Phys.* **2008**, *77*, 085323.
- [6] R. M. Smith, B. Liu, J. Bai, T. Wang, *Appl. Phys. Lett.* **2014**, *105*, 171111.
- [7] F. Bianchi, S. Sadofev, R. Schlesinger, B. Kobin, S. Hecht, N. Koch, F. Henneberger, S. Blumstengel, *Appl. Phys. Lett.* **2014**, *105*, 233301.
- [8] U. Hörmann, S. Zeiske, S. Park, T. Schultz, S. Kickhöfel, U. Scherf, S. Blumstengel, N. Koch, D. Neher, *Appl. Phys. Lett.* **2019**, *114*, 183301.
- [9] F. Piersimoni, R. Schlesinger, J. Benduhn, D. Spoltore, S. Reiter, I. Lange, N. Koch, K. Vandewal, D. Neher, *J. Phys. Chem. Lett.* **2015**, *6*, 500.
- [10] M. Eyer, S. Sadofev, J. Puls, S. Blumstengel, *Appl. Phys. Lett.* **2015**, *107*, 221602.
- [11] J. C. Scott, *J. Vac. Sci. Technol., A* **2003**, *21*, 521.
- [12] M. Riede, T. Mueller, W. Tress, R. Schueppel, K. Leo, *Nanotechnology* **2008**, *19*, 424001.
- [13] S. Park, J. Jeong, G. Hyun, M. Kim, H. Lee, Y. Yi, *Sci. Rep.* **2016**, *6*, 35262.
- [14] I. Lange, S. Reiter, M. Pätzelt, A. Zykov, A. Nefedov, J. Hildebrandt, S. Hecht, S. Kowarik, C. Wöll, G. Heimel, D. Neher, *Adv. Funct. Mater.* **2014**, *24*, 7014.
- [15] S. J. Wilkins, T. Paskova, A. Ivanisevic, *Appl. Surf. Sci.* **2015**, *327*, 498.
- [16] R. Schlesinger, Y. Xu, O. T. Hofmann, S. Winkler, J. Frisch, J. Niederhausen, A. Vollmer, S. Blumstengel, F. Henneberger, P. Rinke, M. Scheffler, N. Koch, *Phys. Rev. B* **2013**, *87*, 155311.
- [17] R. Schlesinger, F. Bianchi, S. Blumstengel, C. Christodoulou, R. Ovsyannikov, B. Kobin, K. Moudgil, S. Barlow, S. Hecht, S. R. Marder, F. Henneberger, N. Koch, *Nat. Commun.* **2015**, *6*, 6754.
- [18] W. Chen, S. Chen, C. Q. Dong, Y. G. Xing, A. T. S. Wee, *J. Am. Chem. Soc.* **2007**, *129*, 10418.
- [19] T. Schultz, R. Schlesinger, J. Niederhausen, F. Henneberger, S. Sadofev, S. Blumstengel, A. Vollmer, F. Bussolotti, J.-P. Yang, S. Kera, K. Parvez, N. Ueno, K. Müllen, N. Koch, *Phys. Rev. B* **2016**, *93*, 125309.
- [20] N. Koch, S. Duhm, J. P. Rabe, A. Vollmer, R. L. Johnson, *Phys. Rev. Lett.* **2005**, *95*, 237601.
- [21] G. Heimel, S. Duhm, I. Salzmann, A. Gerlach, A. Strozecka, J. Niederhausen, C. Bürker, T. Hosokai, I. Fernandez-Torrente, G. Schulze, S. Winkler, A. Wilke, R. Schlesinger, J. Frisch, B. Bröker, A. Vollmer, B. Detlefs, J. Pflaum, S. Kera, K. J. Franke, N. Ueno, J. I. Pascual, F. Schreiber, N. Koch, *Nat. Chem.* **2013**, *5*, 187.
- [22] Y. Zhou, C. Fuentes-Hernandez, J. Shim, J. Meyer, A. J. Giordano, H. Li, P. Winget, T. Papadopoulos, H. Cheun, J. Kim, M. Fenoll, A. Dindar, W. Haske, E. Najafabadi, T. M. Khan, H. Sojoudi, S. Barlow, S. Graham, J. L. Brédas, S. R. Marder, A. Kahn, B. Kippelen, *Science* **2012**, *336*, 327.
- [23] A. Mansour, M. Said, S. Dey, H. Hu, S. Zhang, R. Munir, Y. Zhang, K. Moudgil, S. Barlow, S. Marder, A. Amassian, *Adv. Funct. Mater.* **2017**, *27*, 1602004.
- [24] F. Widdascheck, A. A. Hauke, G. Witte, *Adv. Funct. Mater.* **2019**, *29*, 1808385.
- [25] X. Liu, Y. Zhan, S. Braun, F. Li, M. Fahlman, *Phys. Rev. B: Condens. Matter Mater. Phys.* **2009**, *80*, 115401.
- [26] R. Forker, D. Kasemann, T. Diemel, C. Wagner, R. Franke, K. Müllen, T. Fritz, *Adv. Mater.* **2008**, *20*, 4450.
- [27] T. Katayama, K. Mukai, S. Yoshimoto, J. Yoshinobu, *J. Phys. Chem. Lett.* **2010**, *1*, 2917.
- [28] S. Yoshimoto, K. Kameshima, T. Koitaya, Y. Harada, K. Mukai, J. Yoshinobu, *Org. Electron.* **2014**, *15*, 356.
- [29] H. H. Arefi, G. Fagas, *J. Phys. Chem. C* **2014**, *118*, 14346.
- [30] R. Hunger, C. Pettenkofer, R. Scheer, *J. Appl. Phys.* **2002**, *91*, 6560.
- [31] D. C. Gleason-Rohrer, B. S. Brunshwig, N. S. Lewis, *J. Phys. Chem. C* **2013**, *117*, 18031.
- [32] R. S. Becker, G. S. Higashi, Y. J. Chabal, A. J. Becker, *Phys. Rev. Lett.* **1990**, *65*, 1917.
- [33] F. J. Himpsel, G. Hollinger, R. A. Pollak, *Phys. Rev. B* **1983**, *28*, 7014.
- [34] M. Grundmann, *The Physics of Semiconductors: An Introduction Including Devices and Nanophysics*, Springer, Berlin/Heidelberg **2006**.
- [35] M. Kröger, S. Hamwi, J. Meyer, T. Riedl, W. Kowalsky, A. Kahn, *Appl. Phys. Lett.* **2009**, *95*, 123301.
- [36] S. Winkler, J. Frisch, R. Schlesinger, M. Oehzelt, R. Rieger, J. Räder, J. P. Rabe, K. Müllen, N. Koch, *J. Phys. Chem. C* **2013**, *117*, 22285.
- [37] M. T. Greiner, M. G. Helander, W. M. Tang, Z. Bin Wang, J. Qiu, Z. H. Lu, *Nat. Mater.* **2012**, *11*, 76.
- [38] Y. Qi, T. Sajoto, S. Barlow, E. G. Kim, J. L. Brédas, S. R. Marder, A. Kahn, *J. Am. Chem. Soc.* **2009**, *131*, 12530.
- [39] H. Wang, S. V. Levchenko, T. Schultz, N. Koch, M. Scheffler, M. Rossi, *Adv. Electron. Mater.* **2019**, *5*, 1800891.
- [40] F. Zhang, A. Kahn, *Adv. Funct. Mater.* **2018**, *28*, 1703780.
- [41] J. P. Yang, F. Bussolotti, Y. Q. Li, X. H. Zeng, S. Kera, J. X. Tang, N. Ueno, *Org. Electron.* **2015**, *24*, 120.
- [42] H. Wang, P. Amsalem, G. Heimel, I. Salzmann, N. Koch, M. Oehzelt, *Adv. Mater.* **2014**, *26*, 925.
- [43] M. Oehzelt, N. Koch, G. Heimel, *Nat. Commun.* **2014**, *5*, 4174.
- [44] S. Braun, W. Osikowicz, Y. Wang, W. R. Salaneck, *Org. Electron.* **2007**, *8*, 14.
- [45] A. J. Giordano, F. Pulvirenti, T. M. Khan, C. Fuentes-Hernandez, K. Moudgil, J. H. Delcamp, B. Kippelen, S. Barlow, S. R. Marder, *ACS Appl. Mater. Interfaces* **2015**, *7*, 4320.
- [46] S. Guo, S. Mohapatra, A. Romanov, T. Tatiana, K. Hardcastle, K. Yesudas, C. Risko, J.-L. Bredas, S. Marder, S. Barlow, *Chem. - Eur. J.* **2012**, *18*, 14760.

- [47] A. Kahn, N. Koch, W. Gao, *J. Polym. Sci., Part B: Polym. Phys.* **2003**, *41*, 2529.
- [48] C. Cen, S. Thiel, G. Hammerl, C. W. Schneider, K. E. Andersen, C. S. Hellberg, J. Mannhart, J. Levy, *Nat. Mater.* **2008**, *7*, 298.
- [49] H. Alves, A. S. Molinari, H. Xie, A. F. Morpurgo, *Nat. Mater.* **2008**, *7*, 574.
- [50] W. Bludau, A. Onton, W. Heinke, *J. Appl. Phys.* **1974**, *45*, 1846.
- [51] H. L. Smith, J. T. Dull, E. Longhi, S. Barlow, B. P. Rand, S. R. Marder, A. Kahn, *Adv. Funct. Mater.* **2020**, *30*, 2000328.
- [52] X. Lin, B. Wegner, K. M. Lee, M. A. Fusella, F. Zhang, K. Moudgil, B. P. Rand, S. Barlow, S. R. Marder, N. Koch, A. Kahn, *Nat. Mater.* **2017**, *16*, 1209.
- [53] J.-P. P. Yang, L.-T. T. Shang, F. Bussolotti, L.-W. W. Cheng, W.-Q. Q. Wang, X.-H. H. Zeng, S. Kera, Y.-Q. Q. Li, J.-X. X. Tang, N. Ueno, *Org. Electron.* **2017**, *48*, 172.
- [54] H. Un, S. A. Gregory, S. K. Mohapatra, M. Xiong, E. Longhi, Y. Lu, S. Rigin, S. Jhulki, C. Yang, T. V. Timofeeva, J. Wang, S. K. Yee, S. Barlow, S. R. Marder, J. Pei, *Adv. Energy Mater.* **2019**, *9*, 1900817.